Acid-based geopolymers: Understanding of the structural evolutions during consolidation and after thermal treatments

V. Mathivet, Jenny Jouin, A. Gharzouni, I. Sobrados, H. Celerier, S. Rossignol, M. Parlier

Acid-based geopolymers: understanding of the structural evolutions during consolidation and after thermal treatments

V. Mathivet[1,2], J. Jouin[1,*], A. Gharzouni[1], I. Sobrados[3], H. Celerier[1], S. Rossignol[1] and M. Parlier[2]

[1] *IRCER: Institut de Recherche sur les Céramiques (UMR7315), 12 rue Atlantis, 87068 Limoges Cedex, France.*

[2] *ONERA: Office national d'études et de recherches aérospatiales, 29 Avenue de la Division Leclerc, 92320 Châtillon, France.*

[3]*Instituto de Ciencia de Materiales de Madrid, Consejo Superior de Investigaciones Científicas (CSIC), C/Sor Juana Inés de la Cruz, 3, ES 28049 Madrid, Spain.*

** Corresponding author: tel.:+ 33 (0)5 87 50 23 88, jenny.jouin@unilim.fr*

Keywords: Phosphoric acid; Mechanisms of formation; Metakaolin; XRD; NMR; FTIR; High Temperature.

Abstract

Materials such as ceramic matrix composites are developed for mechanical applications at high temperature, but their cost remains a limitation. Consequently, the use of acid-based geopolymer matrices may be an alternative to reduce costs.

In this study, the sample was prepared from metakaolin and phosphoric acid. FTIR and NMR spectroscopies, XRD and thermal measurements were used to understand the structural evolution of acid-based geopolymers (binders) during consolidation and after thermal treatments.

According to the results, the consolidation of the binder has been divided into four steps: the dissolution of the metakaolin, the polycondensation reactions forming $AlPO_4$ entities and hydrated phases, the breakdown of Si-O-Al bonds with formation of various hydrated silica

networks and finally the completion of the networks. After a thermal treatment at 1000°C, the binder is constituted of $AlPO_4$ phases, quartz and vitreous silica.

1. Introduction

Ceramics are regularly used in high-temperature applications due to their thermal stability. In the aeronautical industry, components are submitted to high thermomechanical constraints [1]. For those applications, ceramic matrix composites are used to increase the tenacity of those ceramics [2]. But those composites (being oxide or non-oxide ceramics [3]) tend to be expensive [3,4] thus geopolymer matrices can be used as a cost-effective solution. However, after thermal treatments, traditional alkali-based geopolymers cannot be used due to the presence of residual alkali cations responsible for the formation of viscous flow and fibers deterioration [5]. Consequently, in order to avoid these problems, acid-based geopolymers appear to be a promising alternative.

Several studies were carried out on acid-based geopolymers with various aluminosilicate sources, different Si/Al ratios and various Al/P ratios [6, 7, [8]]. Optimal mechanical properties were obtained for an Al/P ratio close to 1 [9] and a H_3PO_4 concentration of 10 $mol.L^{-1}$ [10]. According to some authors [11, 12], the consolidated geopolymer is constituted of a tridimensional [Si-O-P-O-Al] network whereas others suggested [7,10] that it is composed of [Si-O-P-O-Si] and $AlPO_4$ networks.

Temperature-dependant studies demonstrated the formation, starting from 250°C, of $AlPO_4$ polymorphs, crystalline SiO_2 and phosphosilicates in the case of high Si/P ratios [12, 13]. Moreover, acid-based geopolymers show good mechanical and thermal properties due to the formation of refractory phases such as $AlPO_4$ (observed in all studies) when increasing temperature. It is thus essential to understand the temperature-dependant structural evolutions of those samples.

This $AlPO_4$ compound, comprised of PO_4^{3-} and AlO_4^{5-} tetrahedrons, can be synthetized by the heat treatment of hydrated aluminophosphate sources extracted from natural materials such as variscite ($AlPO_4.2H_2O$) [14] or from synthetic materials such as $AlPO_4$-H5 usually obtained by sol-gel route [15]. It is also a refractory phase isostructural with silica with many polymorphs, the most common ones being berlinite (hexagonal), cristobalite (triclinic, hexagonal) and tridymite (orthorhombic, cubic) [16]. Those main polymorphs can be differentiated by X-Ray Diffraction (XRD) [17,18,19], Fourier-Transform Infrared (FTIR) [20, 21, 22] and Nuclear Magnetic Resonance (NMR) [23, 24, 25] spectroscopies. Finally, $AlPO_4$ also exists in various hydrated $AlPO_4.xH_2O$ phases which can be characterized by XRD [26, 27] and FTIR spectroscopy [22, 27] as well.

In acid-based geopolymers, the initial reactive mixture is composed of aluminum, silicon and phosphorous sources. To understand the various phases that could crystallize in temperature, the following section presents the different phases that form in glasses constituted of Al_2O_3-SiO_2-P_2O_5 oxides. First, in the binary SiO_2-Al_2O_3, AlO_4^{5-} tetrahedrons are present in the silica network and form the mullite phase at high temperature. Then, in the binary SiO_2-P_2O_5, the silica and phosphate networks develop separately except for high silica concentrations leading to the formation of structures such as SiP_2O_5 [28] that were characterized by FTIR [29, 30] and NMR [31] spectroscopies. In the binary P_2O_5-Al_2O_3, the addition of Al_2O_3 depolymerizes the phosphate glass, breaking the P-O-P bonds in favor of the more stable P-O-Al bonds. For low aluminum concentrations, the presence of Al^{VI} is observed such as in $Al(PO_3)_3$, whereas Al^{IV} is favored for higher concentrations as in $AlPO_4$ [32]. Finally, in the ternary SiO_2-Al_2O_3-P_2O_5, the Al-O-P bonds are formed preferentially due to their higher stability leading to the formation of $AlPO_4$ and silica-rich zones in the material.

Our research focuses on the understanding of the geopolymer formation from metakaolin and diluted phosphoric acid as well as of its structural evolution with increasing temperature.

Those evolutions were characterized by FTIR and ^{27}Al, ^{29}Si and ^{31}P NMR spectroscopies to study the formation of the various networks within the material. Moreover, XRD and thermal analyses were performed to determine the phases formed during the consolidation and after heat treatment.

2. Materials and methods

2.1. Raw materials and sample preparation

The samples were elaborated from the 85 wt%-phosphoric acid produced by VWR and the metakaolin M3 with a Si/Al molar ratio equal to 1 produced by Imerys and studied by Gharzouni *et al.* [33]. First, the phosphoric acid was diluted in distilled water to a concentration of 8.9 $mol.L^{-1}$ and then was mixed with the metakaolin with a P/Al molar ratio equal to 1. The resulting liquid mixture was then cured in a sealed container at room temperature for 21 days until consolidation. The sample was then heat-treated at various temperatures after being grounded in a planetary mill for 40 min at 400 rpm. Low temperature heat treatments (up to 200°C), were carried out for 30 min in a temperature-controlled electronic scale. For higher temperatures, the samples were heat treated in a furnace with a $5°C.min^{-1}$ slope and a 2 h dwelling time.

2.2. Sample characterization

The FTIR spectra of the samples were recorded on a ThermoFicher Scientific Nicolet 380. It was used in ATR mode for characterizing the raw materials and the samples during consolidation. Consolidated and heat-treated binders, mixed in KBr pellets, were measured in transmittance mode. For both modes, the measurements were recorded between 500 and 4000 cm^{-1} with 64 scans and a 4 cm^{-1} resolution. The data were analyzed on the OMNIC software provided by Nicolet Instrument.

The XRD patterns were recorded with a Bruker D8 Advance diffractometer using CuK_α radiation. The acquisitions were carried out with a 2θ-angle varying from 5 to 60° with a step size of 0.02° and an equivalent time per step of 50 s. Analyzing the XRD patterns was performed using the powder diffraction file (PDF) database of the International Center for Diffraction Data to determine the various crystalline phases present in the samples. The deconvolution of the amorphous domes in the consolidating binder was conducted using the Peakoc software [34]. The refinement was done between 5 and 60° using a Voigt function that takes into account the $CuK\alpha_1$ and $CuK\alpha_2$ wavelengths. Furthermore, the continuous background was fitted with a 2^{nd} order polynomial.

The thermal analyses were performed on an SDT Q600 apparatus from TA Instruments. The heat treatment was realized in platinum crucibles under a flow of dry air ($100mL.min^{-1}$) with a $5°C.min^{-1}$ slope up to 1100 °C.

High resolution MAS-NMR analyses were done at room temperature on a Bruker AVANCE-400 spectrometer. 120 scans were carried out in which 10 s intervals between successive accumulations were necessary to minimize saturation effects. Thus, after a $\pi/2$ excitation, ^{31}P, ^{27}Al and ^{29}Si MAS NMR spectra were recorded at 161.98, 104.26 and 79.49 MHz respectively. The chemical shift values for these elements are given relatively to the external 85% H_3PO_4 and $AlCl_3$ aqueous solutions, and $(CH_3)_4Si$. Deconvolutions were then done with Dmfit and the different spectra were fitted with CSA, quad 1^{st} and Gaussian/Lorentzian models for ^{31}P, ^{27}Al and ^{29}Si, respectively. In the end, the reliability factors of the spectral simulations are within 2% of the observed spectra, and chemical shifts and intensities have respective estimated errors of 0.2 ppm and 5% [33].

3. Results and discussion

3.1. Structural evolution during consolidation

a) FTIR study

In order to study the structural evolution of the binder during consolidation, the reactive mixture was characterized by FTIR ATR spectroscopy (Figure 1). Spectra of the metakaolin and the phosphoric acid were added for an easier determination of the various contributions.

The metakaolin spectrum presents a broad band at 1055 cm^{-1} attributed to the asymmetric stretching (ν_{as}) of Si-O-Si bonds. Those Si-O-Si bonds can be linked to the vibrations of the Q^4, Q^3 and Q^2 entities referring to the G. Engelhardt NMR notation: Q^n, n being the number of bridging oxygens [35]. The band at 790 cm^{-1} is assigned to the bending (δ) of Si-O-Si [36].

The spectrum of phosphoric acid displays bands between 3600 and 3200 cm^{-1} due to the OH stretching of water, SiO-H and PO-H, and at 1630 cm^{-1} attributed to the OH bending of water. The bands at 1250, 1150, 990 and 880 cm^{-1} represent the δ P-OH, ν_{as} P-O, ν_s P-O and ν_s P-OH bonds respectively [37]. Consequently, the bands at 970 and 870 cm^{-1} observed in the initial reactive mixture, can be attributed to the phosphate groups (ν_s P-O (Q^0), ν_s P-OH) whereas the band at 775 cm^{-1} is linked to the δ Si-O-Si bonds.

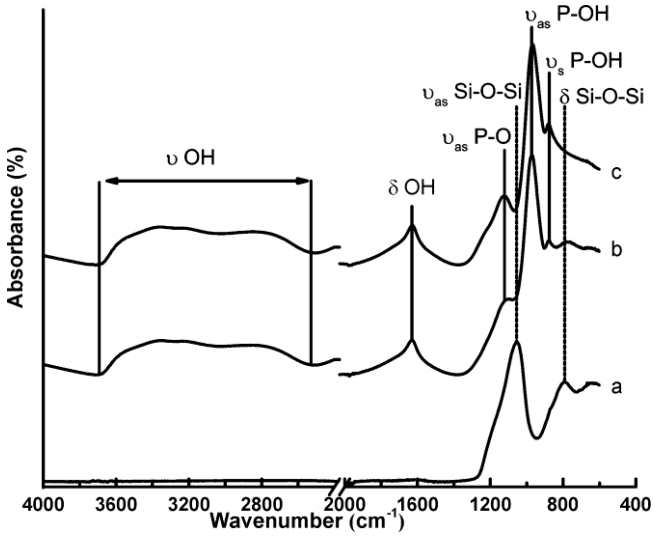

Figure 1: FTIR spectra of the metakaolin (a), the initial reactive mixture (b) and the diluted phosphoric acid (c).

The sample evolution during consolidation was followed by FTIR ATR spectroscopy at various time of consolidation (0, 1, 3, 7, 14 and 20 days) in Figure 2.

The evolution of the hydroxyl groups is presented in Figures 2A and 2B. The initial mixture shows bands at 3553, 3355, 3230, 3154 (clearly visible at day 7) and 2840 cm^{-1} that can be assigned respectively to the following contributions: (i) the ν OH of water molecules for the three first bands, (ii) the hydroxyl vibration of SiO-H [38] and (iii) the ν OH of the phosphoric acid's PO-H [37] (Figure 2A). The evolutions of the intensity of these contributions during consolidation are presented in Figure 2B. In any case, they increase during the first eleven days and then remain constant indicating the presence of hydrated phases from day eleven.

The 1800 to 600 cm^{-1} zone of the spectra are presented in Figure 2A' and 2B'. During the initial stage, the bands measured at 1060 and 800 cm^{-1} are related to the metakaolin (ν_{as} Si-O-Si and δ Si-O-Si) [36] (Figure 2A'). The bands at 970 and 870 cm^{-1} are typical of the phosphoric acid (ν_s P-O, ν_s P-OH) [37]. Between day one and day seven, the intensity of the band at 1050-1100 cm^{-1}, assigned to the ν_s P-O bond from pyrophosphate entities (Q^1), increases while the band at 970 cm^{-1}, attributed to ν_s P-O bond from orthophosphate entities (Q^0), decreases [39]. The intensity of the band at 775 cm^{-1} associated to the δ Si-O-Si bond remains constant. For longer consolidation times, these tendencies remain the same. Moreover, during consolidation, the band ν_{as} P-O-P (900 cm^{-1}) appears and the band ν_s P-OH (880 cm^{-1}) disappears [38].

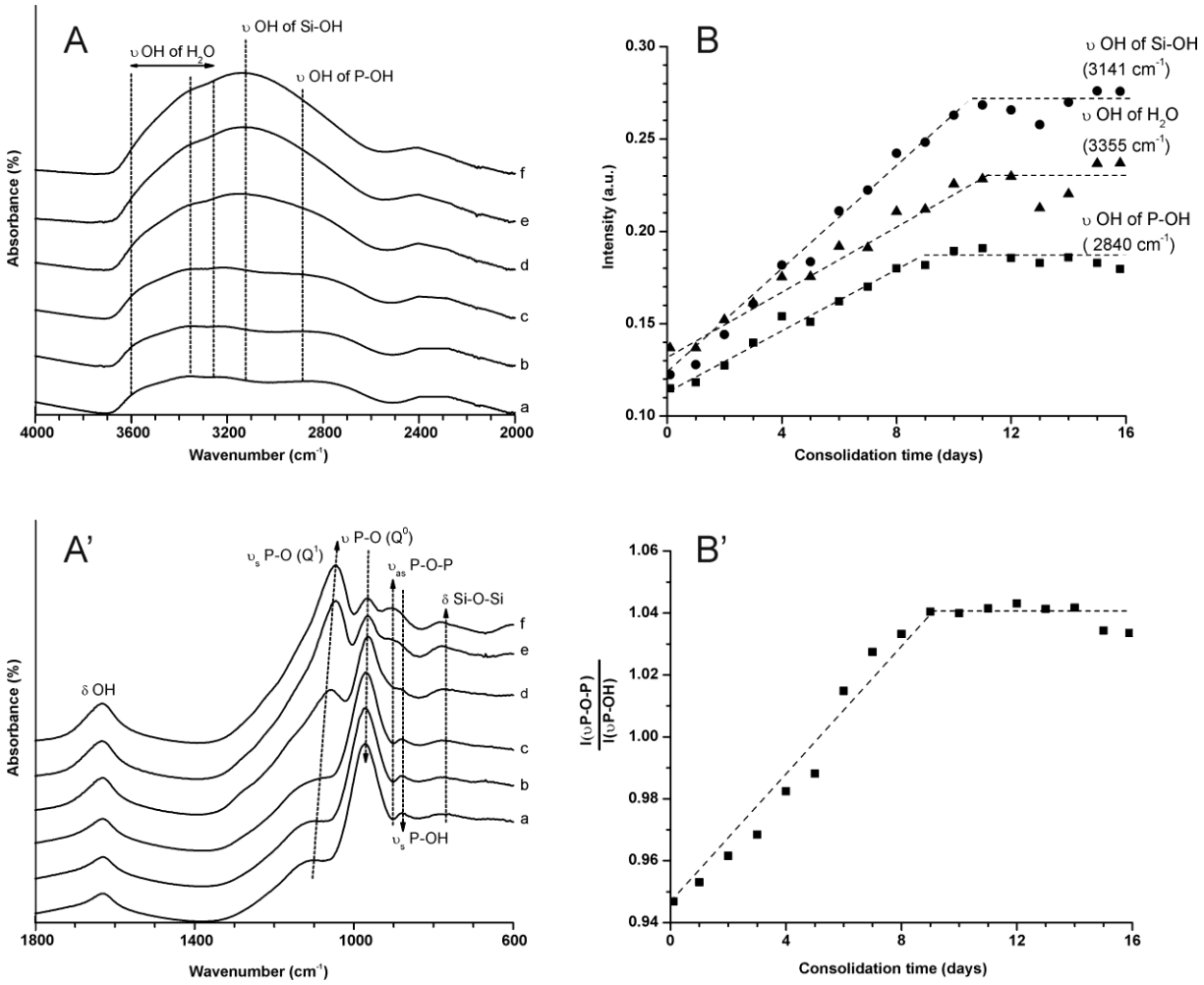

Figure 2: FTIR spectra of the sample measured between (A) 4000-2000 cm^{-1} and (A') 1800-600 cm^{-1} at 0 (a), 1(b), 3(c), 7(d), 14(e) and 20 days (f) of consolidation. (B) evolution of the intensity of v M-OH (M=H, Si and P). (B') evolution of $\frac{\boldsymbol{I\,(\nu_{as}\,P-O-P\ at\ 902\ cm^{-1}})}{\boldsymbol{I\,(\nu_{s}\,P-OH\ at\ 880\ cm^{-1}})}$ as a function of the consolidation time.

In order to study the evolution of those two bands, the evolution of the relative intensity $\frac{\mathrm{I}\,\nu_{\mathrm{as}}\mathrm{P-O-P}}{\mathrm{I}\,\nu_{\mathrm{as}}\mathrm{P-OH}}$ as a function of the consolidation time is presented in Figure 2B'. This relative intensity increases rapidly up to day eleven and reaches a plateau indicating that the P-OH entities polycondensate into P-O-P bonds. Consequently, during consolidation, orthophosphates entities polycondensate to form more polymerized units (Q^1) and hydrated phases.

The polymerized networks formed during consolidation are thus principally constituted of phosphate groups. However, those assignments remain complex due to the presence of silicate species in the same region. Nevertheless, silica-based networks exist in this material.

b) XRD data

To study the evolution of the various networks present in the binder, diffractograms measured at different times of consolidation and the XRD pattern of metakaolin are presented in Figure 3. The latter presents a broad dome centered at 24°, characteristic of its amorphous part and some peaks attributed to crystalline anatase (JCPDS: 01-071-1166) and quartz (JCPDS: 00-046-1045) [40].

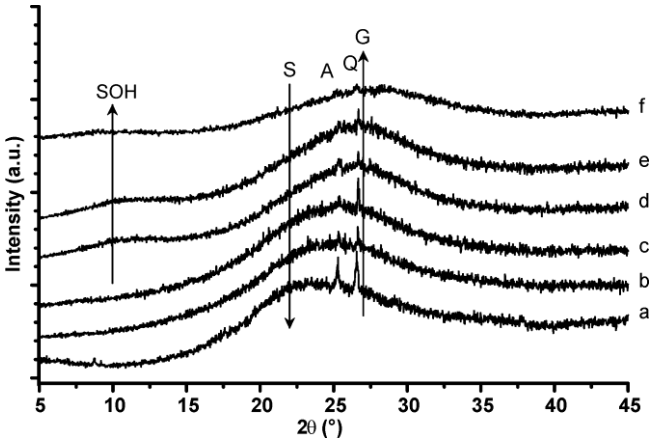

Figure 3: diffractograms of the metakaolin (a), of the binder at days 1(b), 2(c), 8(d) and 9(e) of consolidation and of the consolidated geopolymer (f). In this figure are flagged the positions of anatase (A: 01-071-1166), quartz (Q: 00-046-1045) and of the contributions assigned to hydrated silica (SOH), silica (S) and geopolymer (G) networks.

Whatever the consolidation time, the binder's XRD pattern displays a broad dome at a slightly higher angle of diffraction, typical of amorphous material and the crystalline impurities identified in the metakaolin. However, during consolidation, some minor differences suggest the existence of several contributions. In order to get some more precise information, deconvolutions of the XRD patterns were carried out and the resulting data are gathered in

Table 1. In these calculations, the position of the peak at 21.90°, attributed to pure silica network, was fixed and all the others parameters were refined.

Table 1: deconvolution of the XRD patterns of the binder at various time of consolidation. * fixed parameter

Time (days)	Identified peaks					
	Peak 1 (SOH)		Peak 2 (S)		Peak 3 (G)	
	Position (°) +/-0.01	Relative intensity (%)	Position (°) *	Relative intensity (%)	Position (°) +/-0.01	Relative intensity (%)
1			21.90	27.6	26.49	100
2			21.90	26.7	26.60	100
3			21.90	17.6	26.69	100
4			21.90	11.7	26.62	100
5	6.92	15.8	21.90	10.5	26.47	100
6	8.48	13.7	21.90	8.8	26.59	100
7	8.60	13.9	21.90	7.8	26.67	100
8	10.17	6.2	21.90	7.4	26.56	100
9	10.16	7.4	21.90	6.5	26.72	100
11	9.10	6.4	21.90	4.5	26.86	100
12	8.06	21.3	21.90	3.5	26.81	100
13	8.34	20.5	21.90	3.3	26.79	100
18	8.85	11.7	21.90	3.3	27.01	100
> 21 days	6.48	35.1	21.90	3.4	26.99	100

During the first day of consolidation, the broad dome is constituted of two contributions at 21.90° and 26.49° with relative intensities of 27.6% and 100% respectively. The diffraction line centered at 21.90°, thereafter called S, can be assigned to an amorphous silica network [41] or to an aluminophosphate network [27]. The peak at 26.49°, thereafter called G, which

position is quite constant during geopolymerization, is in agreement with a previous study [6]. It can be attributed to the formation of an amorphous geopolymer network constituted of hydrated aluminophosphates as mentioned by Boonchom and Kongtaweelert [26].

Between day one and day four, the relative intensity of S decreases. At day five, a new diffraction peak appears at around 6.92°, thereafter called SOH, with a relative intensity of 15.8 % and could be attributed to hydrated silica network [42,43]. Between day five and day seven, the relative intensities of SOH and S decrease showing some reorganizations in the associated networks. At day eight, the position of SOH shifts from 8.60° to 10.17° and its relative intensity decreases sharply. That can be linked to a change in hydrated silica. Between day eight and day eleven, the relative intensity of SOH remains constant whereas S's decreases. At day twelve, the position of SOH shifts back to 8.06° and its relative intensity increases strongly. At longer times of consolidation the relative intensities of the S and G contributions remain constant.

In conclusion, this study showed the presence of different types of amorphous networks attributed to hydrated silica, vitreous silica or aluminophosphate and to a geopolymer-like network.

3.2. NMR study at room and high temperature

In order to determine the structural entities, MAS NMR analyses were carried out on the consolidated material after 21 days at room temperature and on a sample heat treated at 1000°C. The ^{31}P, ^{29}Si and ^{27}Al MAS NMR spectra are presented in Figure 4 and the associated deconvolution results are given in Table 2. The assignments of the contributions were not trivial and are based on NMR studies on aluminophosphate and aluminosilicate materials, detailed later for each study. The following notation will be used in the ^{31}P study:

$Q^x(yAl)$ with $\boldsymbol{x}$ the number of phosphorous atoms and $\boldsymbol{y}$ the number of aluminum atoms bonded to a central phosphorous. The same kind of notation will be used in the ^{29}Si study.

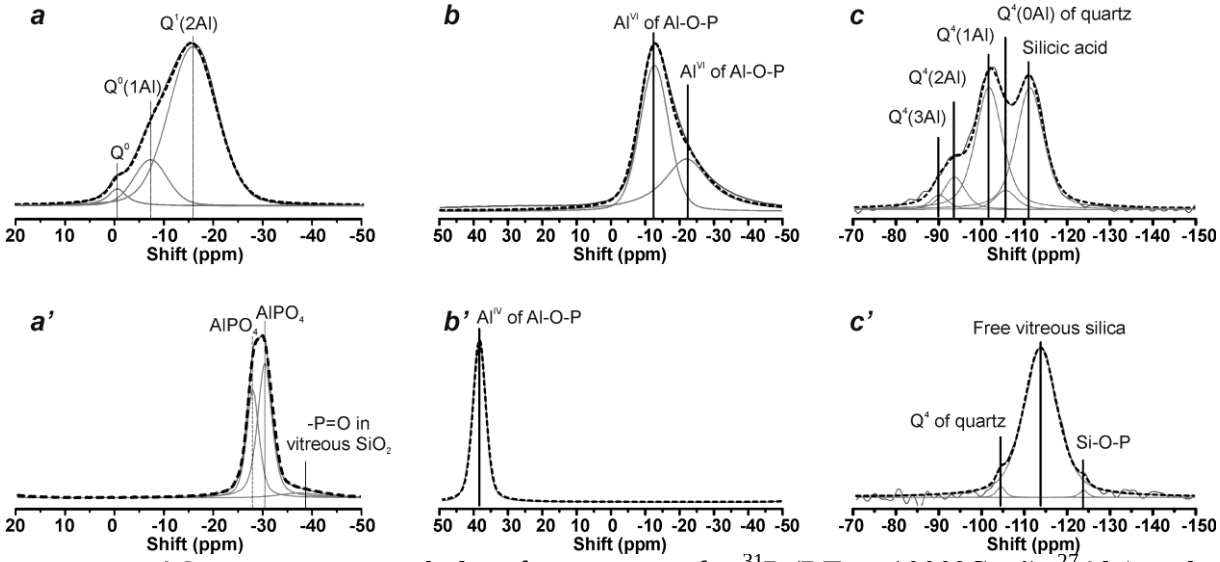

Figure 4: MAS NMR spectra with their fitting curves for ^{31}P (RT: a, 1000°C: a'), ^{27}Al (RT: b, 1000°C: b') and ^{29}Si (RT: c, 1000°C: c').

In the consolidated geopolymer measured at room temperature, the ^{31}P spectrum presents three contributions (with relative intensities) at -0.5 (4.0%), -7.2 (16.0%) and -15.7 ppm (80.0%) attributed to Q^0, $Q^0(1Al)$ and $Q^1(2Al)$ respectively [44,45]. The main contribution (80.0 %) is characteristic of an aluminophosphate network. The ^{27}Al spectrum displays also two contributions at -12.8 (58.3%) and -22.0 ppm (41.7%) that can be assigned to the Al^{VI} in the Al-O-P bond [46, 47]. Those contributions result from the transformation of the metakaolin (containing Al^{VI}, Al^{V} and Al^{IV}). Concerning ^{29}Si, its spectrum presents several contributions at -89.9 (3.2%), -93.5 (5.2%), -101.6 (41.3%), -105.5 (8.8%) and -111.2 ppm (41.6%) assigned to the $Q^4(3Al)$, $Q^4(2Al)$, $Q^4(1Al)$ and $Q^4(0Al)$ of quartz [11, 48] and silicic acid for the last one [49]. These results confirmed the previous XRD and FTIR studies with the observation of two coexisting networks, one being of aluminophosphate and the other of aluminosilicate.

Table 2: deconvolution of MAS NMR ^{31}P, ^{29}Si and ^{27}Al data measured on the binder at room temperature and after a thermal treatment at 1000°C.

		Assignment	Chemical shift (ppm) +/- 0.2 ppm	FWHM (ppm) +/- 5%	Percentage (%)
25°C	^{31}P	Q^0	-0.5	4.5	4.0
		Q^0(1Al)	-7.2	8.0	16.0
		Q^1(2Al)	-15.7	11.5	80.0
	^{27}Al	Al^{VI} of Al-O-P	-12.8	10.0	58.3
		Al^{VI} of Al-O-P	-22.0	16.0	41.7
	^{29}Si	Q^4_{3Al}	-89.9	5.0	3.2
		Q^4_{2Al}	-93.5	6.0	5.2
		Q^4_{1Al}	-101.6	7.5	41.3
		Q^4_{0Al}	-105.5	6.0	8.8
		Silicic acid	-111.2	7.6	41.6
1000°C	^{31}P	$AlPO_4$ of phosphotridymite	-28.1	3.0	37.5
		$AlPO_4$ of phosphocristobalite	-30.6	3.5	53.7
		-P=O in vitreous silica	-37.6	10.0	8.8
	^{27}Al	Al^{IV} of $Al(PO)_4$	39.0	4.4	100
	^{29}Si	Q^4 of quartz	-104.2	2.5	1.8
		Free vitreous silica	-113.6	9.5	97.0
		Si-O-P with Si^{IV}	-123.7	2.5	1.1

The sample treated at 1000°C presents a ^{31}P signal fitted with three contributions at -28.1 (37.5%), - 30.6 (53.7%) and -37.6 ppm (8.8%), the first two being attributed to an $AlPO_4$ phase [24, 25] and the last one to –P=O bonds linked to vitreous silica [50]. The ^{27}Al spectrum also shows a well defined contribution at 39.0 ppm that can be assigned to the Al^{IV} in the $AlPO_4$ phase [23]. The ^{29}Si spectrum presents a broad band with three contributions at -104.2 (1.8%), -113.6 (97.0%) and -123.7 ppm (1.1%), respectively attributed to quartz, free vitreous silica [51, 52] and Si-O-P bonds [53]. After thermal treatment, the binder is constituted of $AlPO_4$ entities and a silica network constituted of quartz and vitreous silica which can be disordered by the inclusion of phosphate ions.

All these data underline that the reaction between metakaolin and phosphoric acid at room temperature leads to the formation of different networks that transform in crystalline $AlPO_4$ and non-crystalline silicate phases at high temperatures. In order to understand what happen during thermal treatment, a study based on thermal analyses, XRD and FTIR will be presented in the following section.

3.3. High temperature induced structural modifications

a) Thermal analyses

Thermal analyses (TG-DTA) were performed on the consolidated material. For the sake of clarity, only the temperature range from 20°C to 240°C is represented in Figure 5. However, it is to be noted that at 980°C the observation of a small exothermic peak was assigned to the formation of mullite [54, 55].

In the low-temperature range, a broad endothermic phenomenon is attributed to water loss. In order to better determine the various amounts of water released in this range, the Figure 5 also presents the derivative of the weight loss as a function of temperature. Thus, four steps can be identified and will be named I, II, III, IV, corresponding to T < 100°C, 100°C < T < 115°C,

115°C < T < 150°C and 150°C < T < 230°C respectively. An important weight loss of 17% is observed for step I and represents the departure of physisorbed water. The other three weight losses relative to steps II, III and IV are 7.0, 3.0 and 1.5% respectively and correspond to the loss of hydrated phases. Consequently, those weight losses for the temperature range 100°C-230°C are due to metastable phases that can be linked to hydrated aluminophosphates.

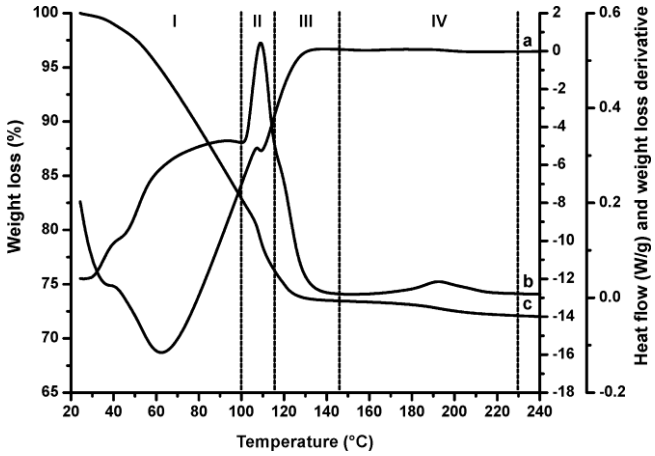

Figure 5: thermal analysis of the geopolymer ((a) heat flow, (b) weight loss and (c) weight loss derivative) shown between 20 and 240 °C.

b) XRD study

To better identify the sample's structure, XRD patterns were recorded after thermal treatment at various temperatures (Figure 6). The consolidated binder presents a main dome centered at 26.99° typical of the geopolymer network. At temperatures of 50°C and 90°C, this amorphous dome shifts towards lower angles, due to a slight structural reorganization of the material. At 110°C, the main reflections at 20.44° and 21.76° are attributed to a preponderant $AlPO_4$ cristobalite (O) (040) plane [17] and a minor $AlPO_4$ tridymite (T) (111) plane [18], respectively. Moreover, several diffraction peaks, clearly visible at 130°C, appear at 11.47° and 21.79° and correspond to hydrated aluminophosphates (Hy) [26]. At 150°C, a peak characteristic of the $AlPO_4$ berlinite (H) (012) plane [19] appears at 26.42°. At 200°C, the hydrated aluminophosphates disappear, which is coherent with the complete water loss

observed by TG-DTA. Between 200°C and 500°C, the berlinite reflections intensities increase to the detriment of the cristobalite and tridymite ones disappearing at 500°C. Furthermore, at 1000°C, the tridymite and cristobalite $AlPO_4$ phases reappear with the tridymite phase being the major contribution, whereas the berlinite form disappears.

Consequently, the increase in temperature modifies the geopolymer's structure with major evolutions at medium temperature (90°C to 200°C). Also, we observed the temperature-dependent existence of three different $AlPO_4$ polymorphs in the material.

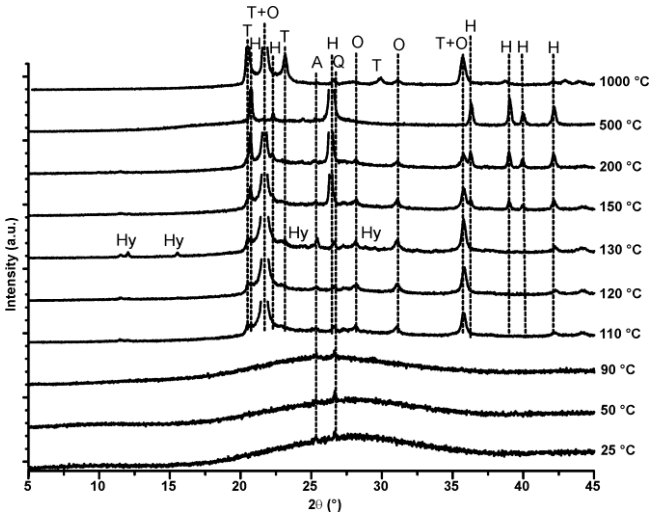

Figure 6: XRD patterns of the sample treated at various temperatures. In this figure are flagged the positions T: trydimite-type $AlPO_4$ (01-070-4689), O: cristobalite-type $AlPO_4$ (01-072-1161), H: berlinite $AlPO_4$ (01-089-4201), Hy: hydrated aluminophosphate such as $Al(H_2PO_4)_3$ (01-14-0377) and $Al(H_2PO_4)(HPO_4)H_2O$ (00-76-376), A: anatase (01-071-1166) and Q: quartz (00-046-1045).

c) FTIR study

FTIR analyses were conducted to study the structural evolution of the geopolymer during heat treatment. The spectra are given as a function of temperature in Figure 7.

The hydroxyl groups' contributions are presented in Figure 7A. At room temperature the bands located at 3530, 3350, 3240 and 3140 cm^{-1} are attributed to the ν OH of water molecules for the first three and to ν OH of SiO-H for the last one. With increasing

temperature, all these contributions decrease and disappear after 200°C, due to the dehydration of the sample.

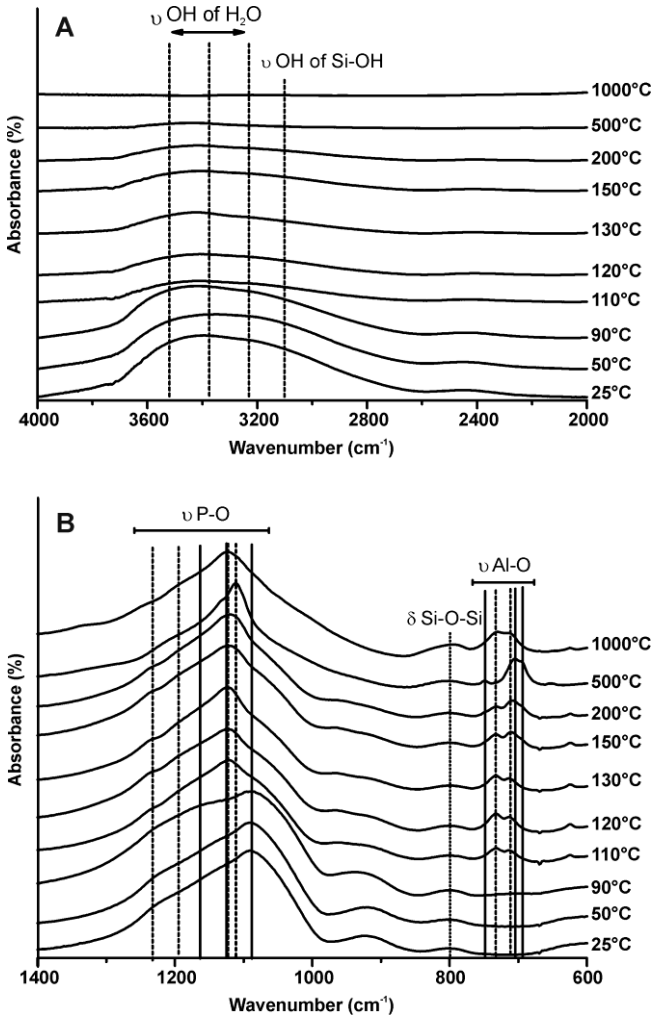

Figure 7: FTIR spectra of the sample measured at various temperatures between 4000-2000 cm^{-1} (A) and 1400-600 cm^{-1} (B) with the main positions of (-) $AlPO_4$ hydrated, (-) $AlPO_4$ berlinite, (--) $AlPO_4$ tridymite and cristoballite, (..) δ Si-O-Si.

The 1800 to 600 cm^{-1} parts of the spectra are presented in Figure 7B. At room temperature, contributions at 1220 (w), 1155 (w), 1095 and 920 cm^{-1} are typical of stretching P-O bands of hydrated aluminophosphate [22, 27]. The bands corresponding to Si-O-Si species (Q^4, Q^3, Q^2, Q^1) are overlapped by the P-O contributions and only the bending of Si-O-Si is detected at 800 cm^{-1}. At 110°C, additional bands appear at 1230, 1180 cm^{-1} (ν P-O), 730 and 715 cm^{-1} (ν Al-O) attributed to $AlPO_4$ with tridymite- and cristobalite-like structures [20, 21]. Moreover,

the contribution located at 1130 cm^{-1} can be assigned to the ν P-O of all $AlPO_4$ polymorphs [20, 22]. In the temperature range 110°C-200°C, bands at 1114 cm^{-1} (ν P-O), 750, 705 and 698 cm^{-1} (ν Al-O) are attributed to $AlPO_4$ berlinite [20, 22]. At 500°C, only the bands relative to the $AlPO_4$ berlinite are predominant and those of $AlPO_4$ tridymite and cristobalite disappear. At 1000°C, the bands characteristic of $AlPO_4$ tridymite and cristobalite reappear due to the recrystallization of those phases, while the bands of $AlPO_4$ berlinite are absent.

This evolution in temperature confirms the presence of hydrated phases at room temperature and a mixture of $AlPO_4$ phases (berlinite, cristobalite and tridymite) after thermal treatment. Moreover, those data prove the existence of aluminophosphate nuclei, which is in agreement with the previous study of the geopolymer consolidation.

4 Discussion

All data corroborate the presence of several silica- and aluminophosphate-based networks as well as hydrated phases in the consolidated geopolymer. The presence of aluminophosphate is indeed confirmed by the XRD study (diffraction peak at 27°), the NMR study (presence of Al-O-P bonds for ^{27}Al and of Q^0(1Al) and Q^1(2Al) entities for ^{31}P) and the characterizations after heat treament demonstrating the presence of $AlPO_4$ nuclei. Moreover, the presence of hydrated aluminophosphate was shown by thermal analyses, FTIR and XRD. Finally, the existence of amorphous silica and hydrated silica networks is confirmed by NMR (presence of Q^4(0Al) and silicic acid for ^{29}Si) and XRD studies (diffraction peaks at 8° and 21.90°).

In order to investigate the binder's formation in acidic medium, the dissolution step of the metakaolin and the behavior of the phosphate entities must be understood. Thus, the evolution of $\frac{I\ \nu\ P{-}O\ Q^1}{I\ \nu\ P{-}O\ Q^0}$ and $\frac{I_G}{I_S}$ as a function of the consolidation time is shown in Figure 8. The $\frac{I\ \nu\ P{-}O\ Q^1}{I\ \nu\ P{-}O\ Q^0}$ ratio is defined by the intensities of the ν P-O Q^1 (1045 cm^{-1}) and ν P-O Q^0 (970 cm^{-1}) bands extracted from FTIR, and represents the polycondensation of the phosphate network. The $\frac{I_G}{I_S}$

ratio is defined by the intensities of the XRD contributions at 21.9° (I_S) and at around 27° (I_G), and depicts the formation of the geopolymer network to the detriment of the amorphous silica network.

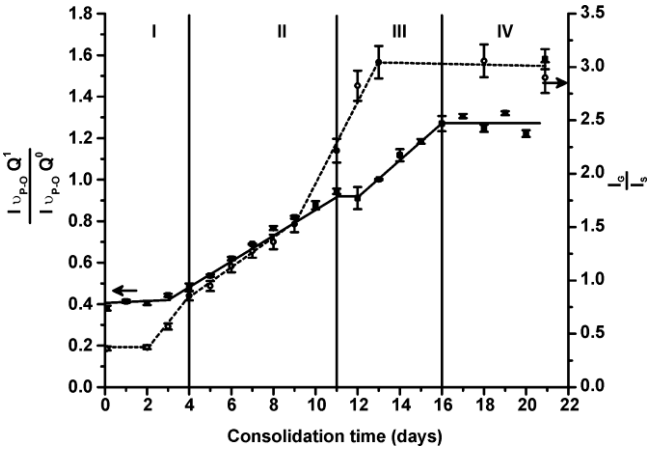

Figure 8: evolutions of the $\frac{I\,\upsilon\,P{-}O\;Q^1\;(1045\;cm^{-1})}{I\,\upsilon\,P{-}O\;Q^0\;(970\;cm^{-1})}$ ratio from FTIR spectra (black squares) and of the $\frac{I_G}{I_S}$ ratio from XRD patterns (open circles) as a function of the consolidation time.

Both ratios follow the same pattern, with an increase of their value up to 14 days before reaching a plateau, indicating the formation of polymerized entities including disordered Al-O-P networks. After a careful examination, the variation of the curves allows to divide the polymerization process into four zones represented in Figure 8. The dissolution of the metakaolin and the equilibrium speciation of H_3PO_4 [37] take place in zone I (up to day 4). As a matter of fact, in alkaline medium, the dissolution of the metakaolin leads to the release of aluminum and silica. However, in acidic medium, only the aluminum is able to solubilize whereas it is very difficult for the silica [56, 57]. Consequently, during the dissolution step, only Al^{3+} and a few silica are in contact with PO_4^{3-} entities in the medium. The dissolution of the metakaolin can also lead to the formation of some Al^{3+} linked to unreacted silica. This phenomenon is supported by the slight variation of the $\frac{I\,\upsilon\,P{-}O\;Q^1}{I\,\upsilon\,P{-}O\;Q^0}$ and $\frac{I_G}{I_S}$ ratios, and the limited

disappearance of PO_4^{3-} entities highlighted by the decrease of the intensity of the ν PO (Q^0) band in FTIR.

In zone II (from day 4 to day 11), both ratios increase rapidly meaning that the polycondensation clearly begins. Moreover, zone II sees the formation of hydrated phases. The FTIR study corroborates the presence of hydroxyl groups and the increase of the intensity of ν Si-OH (3152 cm^{-1}), whereas the XRD study shows the appearance of $Si(OH)_4$ (diffraction peak at ~ 8°). It demonstrates that some unreacted silica is hydrolyzed in the medium.

In zone III (from day 11 to day 16), the increase of $\frac{I\ \nu\ P{-}O\ Q^1}{I\ \nu\ P{-}O\ Q^0}$ and $\frac{I_G}{I_S}$ (until day 13) depicts the polycondensation reactions of phosphate entities, forming an aluminophosphate network as evidenced by the crystallization of $AlPO_4$ nuclei in the temperature dependent XRD study. The formation of $AlPO_4$ suggests that the bonds between Si-O-Al have been broken to release Al^{3+} and Si^{4+}. Furthermore, the diffraction peak attributed to hydrated silica shifts from 10° to 8° while its intensity increases. All these observations lead to the fact that silica species released in solution are able to react with the other silica available to form a new $Si(OH)_4$ network.

In zone IV (from day 16 to day 21), $\frac{I_G}{I_S}$ remains constant, which suggests that the local order does not evolve. In parallel, $\frac{I\ \nu\ P{-}O\ Q^1}{I\ \nu\ P{-}O\ Q^0}$ only presents a slight variation, indicating that the polycondensation reactions are also finishing. This variation reveals that the various local networks are formed in agreement with the several phases observed when increasing temperature. Consequently, the consolidation mechanism can be divided into four steps resulting in the formation of an Al-O-P network (NMR ^{31}P (-7.2, -15.7 ppm) and ^{27}Al (-12.8, -22.0 ppm)) and a silica gel (NMR ^{29}Si (-105.5, -111.2 ppm)) with some remaining Si-O-Al bonds (NMR ^{29}Si (-89.9, -93.5, -101.6 ppm)).

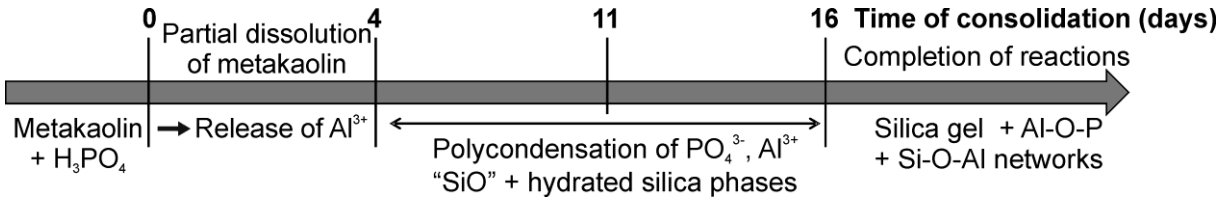

Figure 9: summary of the geopolymer's formation mechanism.

5. Conclusion

This study is focused on the understanding of the geopolymer formation process and its structural evolution after thermal treatments. During consolidation, the formation of polymerized phosphate networks and hydrated phases was conclusively proved by FTIR. The various amorphous networks (hydrated silica, silica and geopolymer) were evidenced by XRD with the decrease in the amount of silica in favor of the formation of hydrated silica and geopolymer networks. All of this was confirmed by NMR measurements.

The formation of the geopolymer network can be separated into four steps summarized in Figure 9. The thermal treatment of the binder at 1000°C leads to the formation of various $AlPO_4$ polymorphs, quartz and amorphous silica already present in the sample. Thus, this material could be used for high-temperature applications due to the formation of stable and refractory phases at high temperature.

References

[1] H. Ohnabe, S. Masaki, M. Onozuka, K. Miyahara, T. Sasa, Composites Part A 30 (1999) 489-496.

[2] K.G. Dassios, Adv. Compos. Lett. 16 (2007) 17-24.

[3] R.W.Davidge, Composite Materials Series 6 (1989) 547-569.

[4] M. Rosso, J. Mater. Process. Technol. 175 (2006) 364-375.

[5] M.K. Cinibulk, R.S. Hay, J. Am. Ceram. Soc. 79 (1996) 1233-1246.

[6] H.K. Tchakouté, C.H. Rüscher, Appl. Clay. Sci. 140 (2017) 81-87.

[7] S. Louati, S. Baklouti, B. Samet, Appl. Clay. Sci., vol. 132–133 (2016) 571-578.

[8] H. Celerier, J. Jouin, V. Mathivet, N. Tessier-Doyen, S. Rossignol, J. Non-Cryst. Solids, 493, 2018, 94-98

[9] H. Douiri, S. Louati, S. Baklouti, M. Arous, Z. Fakhfakh, Mater. Lett. 116 (2014) 9-12.

[10] H.K. Tchakouté, C.H. Rüscher, E. Kamseu, F. Andreola, C. Leonelli, Appl. Clay. Sci. 147 (2017) 184-194.

[11] D.S. Perera, J.V. Hanna, J. Davis, M.G. Blackford, B.A. Latella, Y. Sasaki, E.R. Vance, J. Mater. Sci. 43 (2008) 6562-6566.

[12] L. Le-ping, C. Xue-Min, H. Yan, L. Si-dong, G. Si-yu, Mater. Lett. 66 (2012) 10-12.

[13] M. Khabbouchi, K. Hosni, M. Mezni, C. Zanelli, M. Doggy, Appl. Clay. Sci. 146 (2017) 510-516.

[14] A.M. Arjona, M.A. Alario Franco, J. Therm. Anal. 5 (1973) 319-328.

[15] W. Mekky, P.S. Nicholson, J. Mater. Process. Technol. 190 (2017) 393-396.

[16] H.A. Graetsch, Z. Kristallogr. 222 (2007) 226-233.

[17] R.C.L. Mooney, Acta Cristallogr. 9 (1956) 728-734.

[18] H.A. Graetsch, Acta Cristallogr., Sect.C 56 (2000) 401-403.

[19] R. Brill, A. Debretteville, Acta Cristallogr. 8 (1955) 567-570.

[20] M. Rokita, M. Handke, W. Mozgawa, J. Mol. Struct. 450 (1998) 213-217.

[21] N.V. Chukanov, A.D. Chervonnyi, "Infrared Spectroscopy of Minerals and Related Compounds", SpringerMineralogy (2016), Springer International Publishing Switzerland.

[22] R. Frost, R. Scholz, F. Belotti, A. López, F. Theiss, Spectrochimi. Acta, Part A 147 (2015) 185-192.

[23] Y. Xiao, R.J. Kirkpatrick, J. Mater. Res. 10 (1995) 2586-2591.

[24] B. Peplinski, B. Adamczyk, P. Formanek, C. Meyer, O. Krüger, H. Scharf, S. Reinsch, M. Ostermann, M. Nofz, C. Jäger, C. Adam, F. Emmerling, ICDD 32 (2017) S193-S200.

[25] R. Xu, W. Zhang, J. Xu, Z. Tian, F. Deng, X. Han, X. Bao, J. Phys. Chem. 117 (2013) 5848-5854.

[26] F. d'Yvoire, Bull. Soc. Chim. Fr (1961) 1762-1776.

[27] B. Boonchom, S. Kongtaweelert, J. Therm. Anal. Calorim. 99 (2010) 531-538.

[28] R. Dupree, J. Non-Cryst. Solids 112 (1989) 111-119.

[29] Y Cao, C. Shao, F. Wang, W. Xu, S. Wang, L. Hu, C. Yu., J. Non-Cryst. Solids 481 (2018) 164-169.

[30] M. Kamal, I.K. Battisha, M.A. Salem, A.M.S. El Nahrawy, J. Sol-Gel Sci. Technol. 58 (2011) 507-517.

[31] C. Coelho, T. Azais, L. Bonhomme-Coury, J. Maquet, D. Massiot, C. Bonhomme, J. Magn. Reson. 179 (2006) 114-119.

[32] E.E. Metwalli, R.K. Brow, F.S. Stover, J. Am. Ceram. Soc. 84 (2001) 1025-1032.

[33] A. Gharzouni, I. Sobrados, E. Joussein, S. Baklouti, S. Rossignol, J. Ceram. Sci. Technol. 8 (2017) 365-376.

[34] O. Masson, PEAKOC profile fitting software v1.0, 2006, access at http://www.esrf.eu/Instrumentation/software/data-analysis/OurSoftware/PEAKOC.

[35] E. Lippmaa, J. Am. Chem. Soc. 102 (1980) 4889-4893.

[36] A. Autef, E. Joussein, G. Gasgnier, S. Rossignol, J. Non-Cryst. Solids 358 (2012) 2286-2893.

[37] J. Baril, J.J. Max, C. Chapados, Can. J. Chem. 78 (2000) 490-507.

[38] A. Bertoluzza, C. Fagnano, M. A. Morelli, V. Gottardi, M. Guglielmi, J. Non-Cryst. Solids 48 (1982) 117-128.

[39] K. Jha, O. Pandey, K. Singh, J. Mol. Struct. 1083 (2015) 278-285.

[40] A. Gharzouni, L. Vidal, N. Essaidi, E. Joussein, S. Rossignol, Mater. Des. 94 (2016) 221-229.

[41] P. Deshmuk, J. Bhatt, D. Peshwe, S. Pathak, Trans. Indian. Inst. Met. 65 (2012) 63-70.

[42] M.D. Shannon, J.L. Casci, P.A. Cox, S.J. Andrews, Nature 353 (1991) 417-420.

[43] L. Guth, D. Jordan, A. Kalt, B. Perati, R. Wey, C.R. Acad. Sc. Paris 285 (1977) 1367-1370.

[44] L. Von Wullen, G. Tricot, S. Wegner, Solid State Nuclear Magnetic Resonance 32 (2007) 44-52.

[45] S. Wegner, L. Von Wullen, G. Tricot, J. Non-Cryst. Solids 354 (2008) 1703-1714.

[46] G.D. Cody, B. Mysen, G. Sághi-Szabó, J.A. Tossell, Geochim. Cosmochim. Acta 65 (2001) 2395-2411.

[47] Y. He, L. Liu, L. He, X. Cui, Ceram. Int. 42 (2016) 10908-10912.

[48] L.H. Merwin, A. Sebald, H. Rager, H. Schneider, Phys. Chem. Minerals 18 (1991) 47-52.

[49] A. Autef, E. Joussein, A. Poulesquen, G. Gasgnier, S. Proniere, I. Sobrados, J. Sanz, S. Rossignol, J. Colloid Interface Sci. 408 (2013) 43-53.

[50] S.G. Kosinski, D.M. Krol, T.M. Duncan, D.C. Douglass, J.B. MacChesney, J.R. Simpson, J. Non-Cryst. Solids 105 (1988) 45-50.

[51] R.H. Meinhold, K.J.D. MacKenzie, I.W.M. Brown, J. Mat. Sci. Lett. 4 (1985) 163

[52] I. Jaymes, A. Douy, P. Florian, D. Massiot, J.P. Coutures, J. Sol-Gel Sci. Technol. 2 (1994) 367-370.

[53] S.P. Szu, L.C. Klein, M. Greenblatt, J. Non-Cryst. Solids, 143 (1992) 21-30.

[54] O. Castelein, B. Soulestin, J.P. Bonnet, P. Blanchart, Ceram. Int. 27 (2001) 517-522.

[55] D. Li, W. Thomson, J. Mater. Res.5 (1990) 1963-1969.

[56] H. Hihara, R.P. Adler, R.M. Latanision, « Environmental Degradation of Advanced and Traditional Engineering Materials », , CRC press (2014) p494-495.

[57] G.B. Alexander, W.M. Heston, R.K. Iler, J. Phys. Chem. 58 (1954) 453-455.

Table 1

Table 1: deconvolution of the XRD patterns of the binder at various time of consolidation.

* fixed parameter

Time (days)	Identified peaks					
	Peak 1 (SOH)		Peak 2 (S)		Peak 3 (G)	
	Position (°) +/-0.01	Relative intensity (%)	Position (°) *	Relative intensity (%)	Position (°) +/-0.01	Relative intensity (%)
1			21.90	27.6	26.49	100
2			21.90	26.7	26.60	100
3			21.90	17.6	26.69	100
4			21.90	11.7	26.62	100
5	6.92	15.8	21.90	10.5	26.47	100
6	8.48	13.7	21.90	8.8	26.59	100
7	8.60	13.9	21.90	7.8	26.67	100
8	10.17	6.2	21.90	7.4	26.56	100
9	10.16	7.4	21.90	6.5	26.72	100
11	9.10	6.4	21.90	4.5	26.86	100
12	8.06	21.3	21.90	3.5	26.81	100
13	8.34	20.5	21.90	3.3	26.79	100
18	8.85	11.7	21.90	3.3	27.01	100
> 21 days	6.48	35.1	21.90	3.4	26.99	100

Table 2

Table 1: deconvolution of MAS NMR ^{31}P, ^{29}Si and ^{27}Al data measured on the binder at room temperature and after a thermal treatment at 1000°C.

		Assignment	Chemical shift (ppm) +/- 0.2 ppm	FWHM (ppm) +/- 5%	Percentage (%)
25°C	^{31}P	Q^0	-0.5	4.5	4.0
		Q^0(1Al)	-7.2	8.0	16.0
		Q^1(2Al)	-15.7	11.5	80.0
	^{27}Al	Al^{VI} of Al-O-P	-12.8	10.0	58.3
		Al^{VI} of Al-O-P	-22.0	16.0	41.7
	^{29}Si	Q^4_{3Al}	-89.9	5.0	3.2
		Q^4_{2Al}	-93.5	6.0	5.2
		Q^4_{1Al}	-101.6	7.5	41.3
		Q^4_{0Al}	-105.5	6.0	8.8
		Silicic acid	-111.2	7.6	41.6
1000°C	^{31}P	$AlPO_4$ of phosphotridymite	-28.1	3.0	37.5
		$AlPO_4$ of phosphocristobalite	-30.6	3.5	53.7
		-P=O in vitreous silica	-37.6	10.0	8.8
	^{27}Al	Al^{IV} of $Al(PO)_4$	39.0	4.4	100
	^{29}Si	Q^4 of quartz	-104.2	2.5	1.8
		Free vitreous silica	-113.6	9.5	97.0
		Si-O-P with Si^{IV}	-123.7	2.5	1.1

Figure 1

Click here to download high resolution image

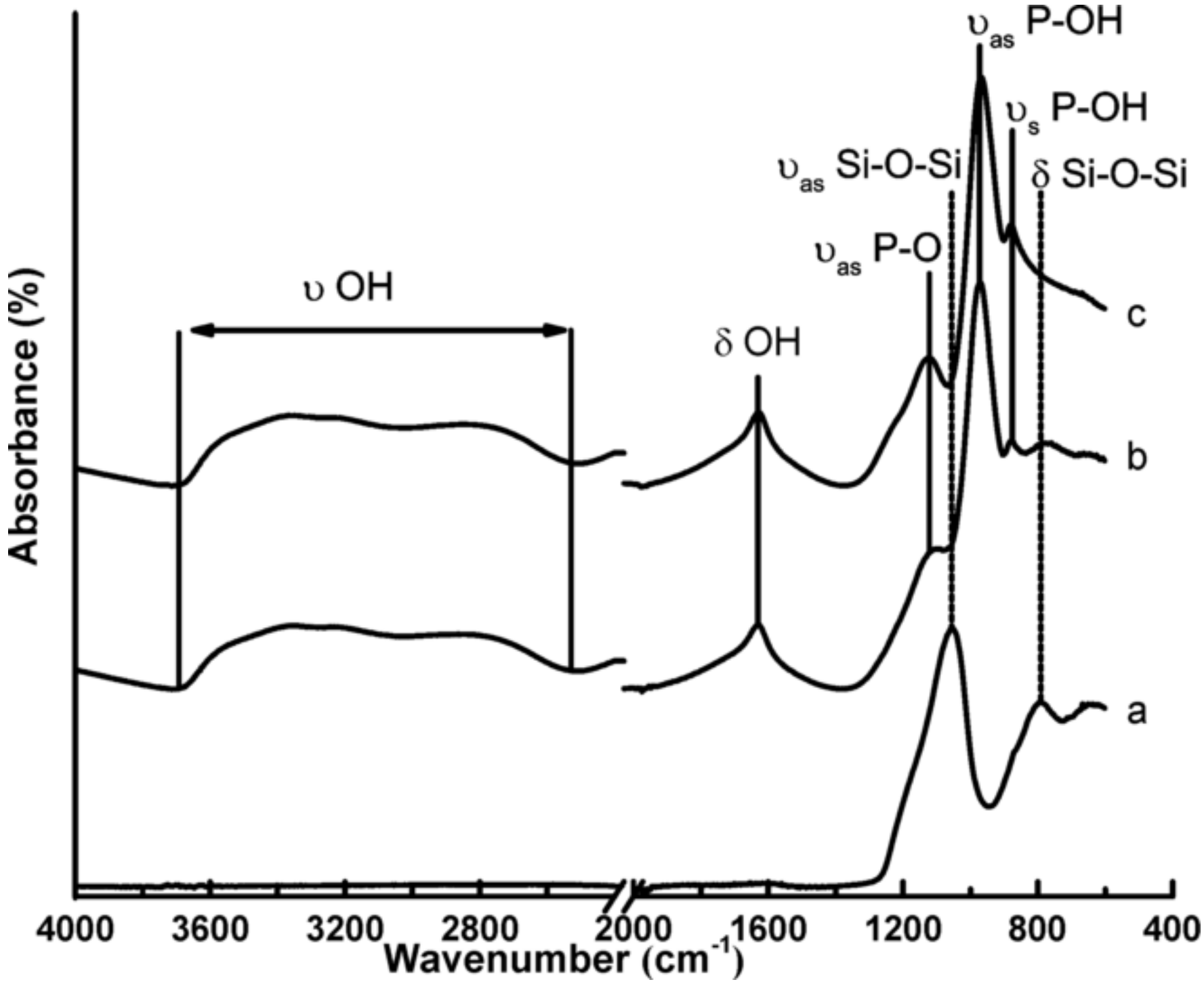

Figure 2

Click here to download high resolution image

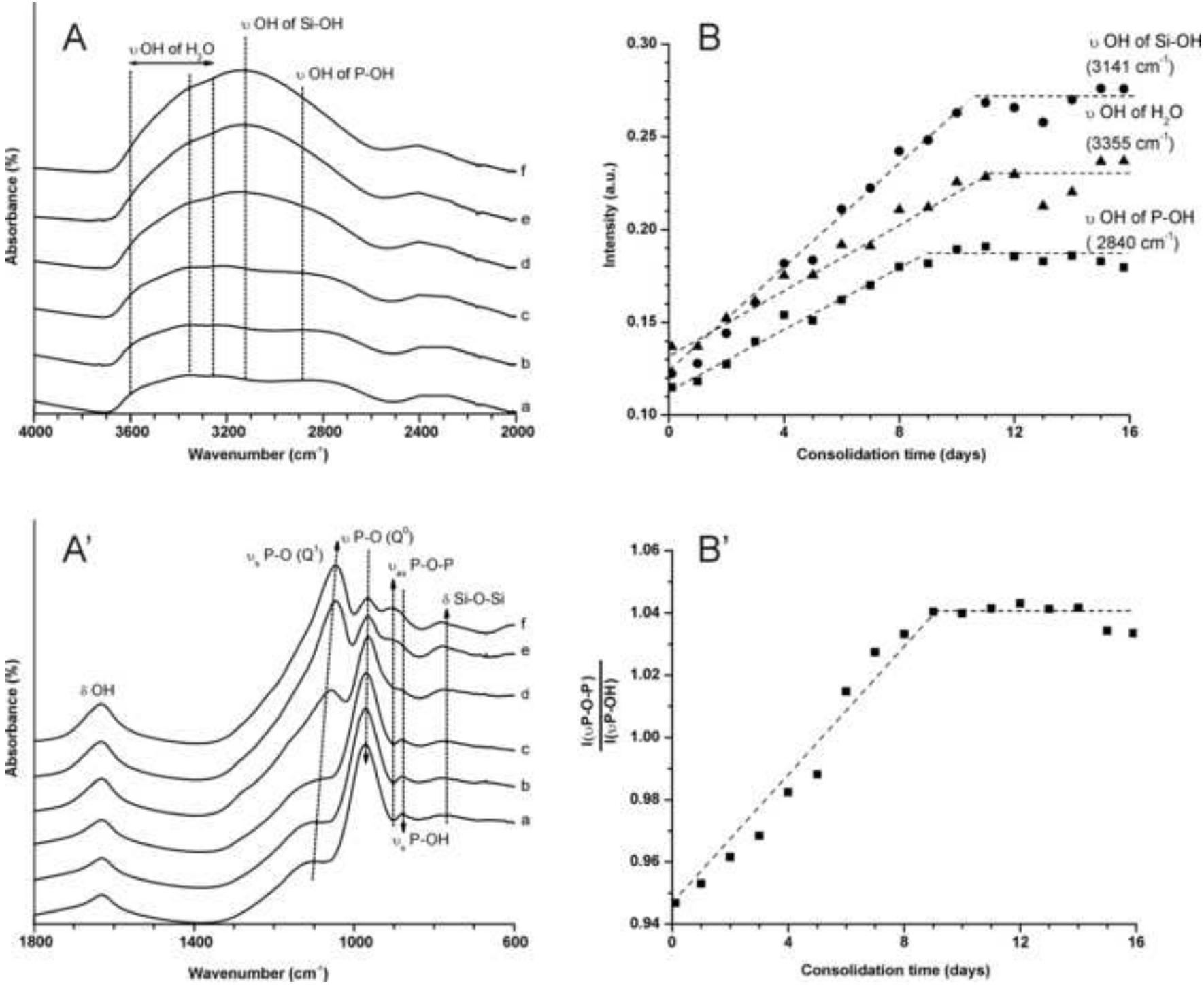

Figure 3

Click here to download high resolution image

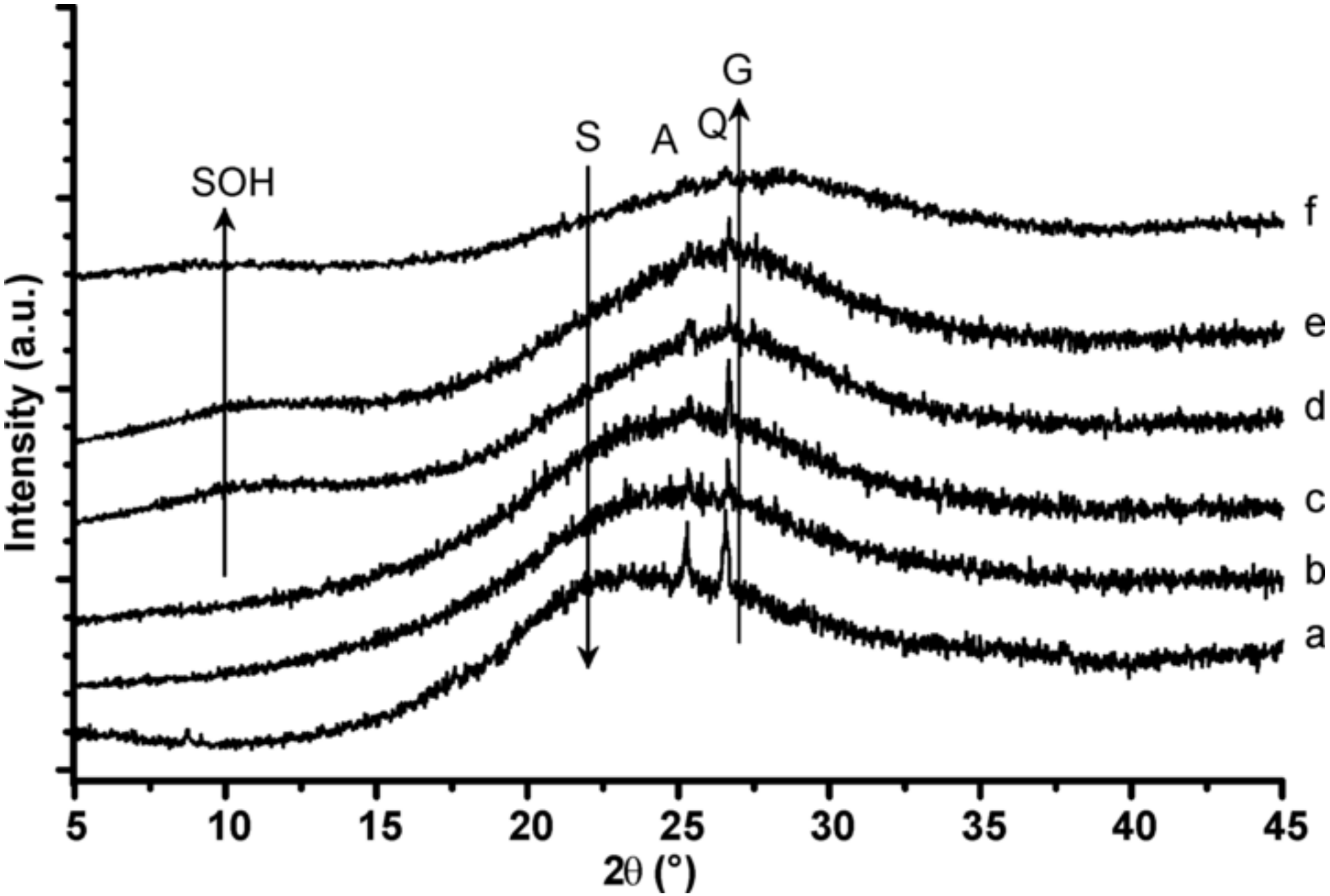

Figure 4

Click here to download high resolution image

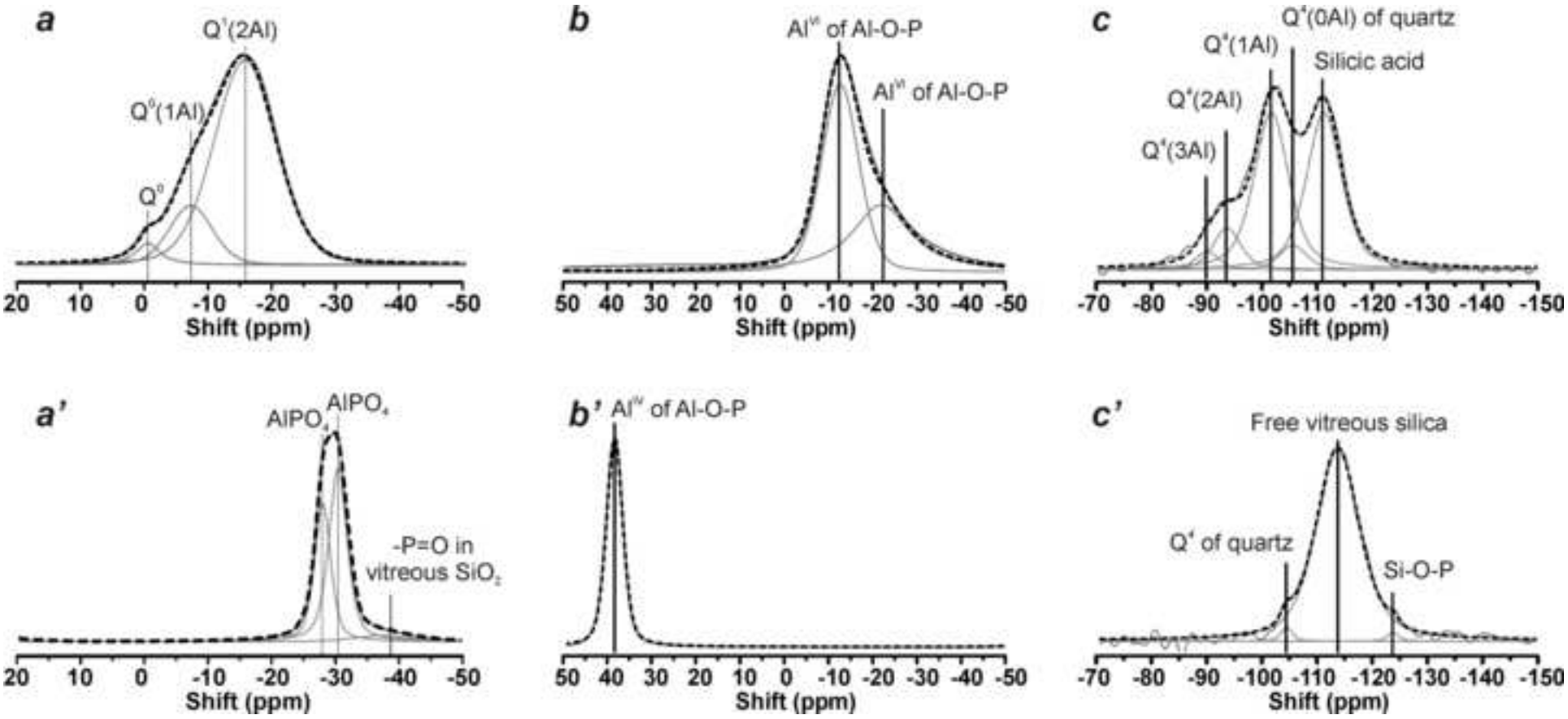

Figure 5

Click here to download high resolution image

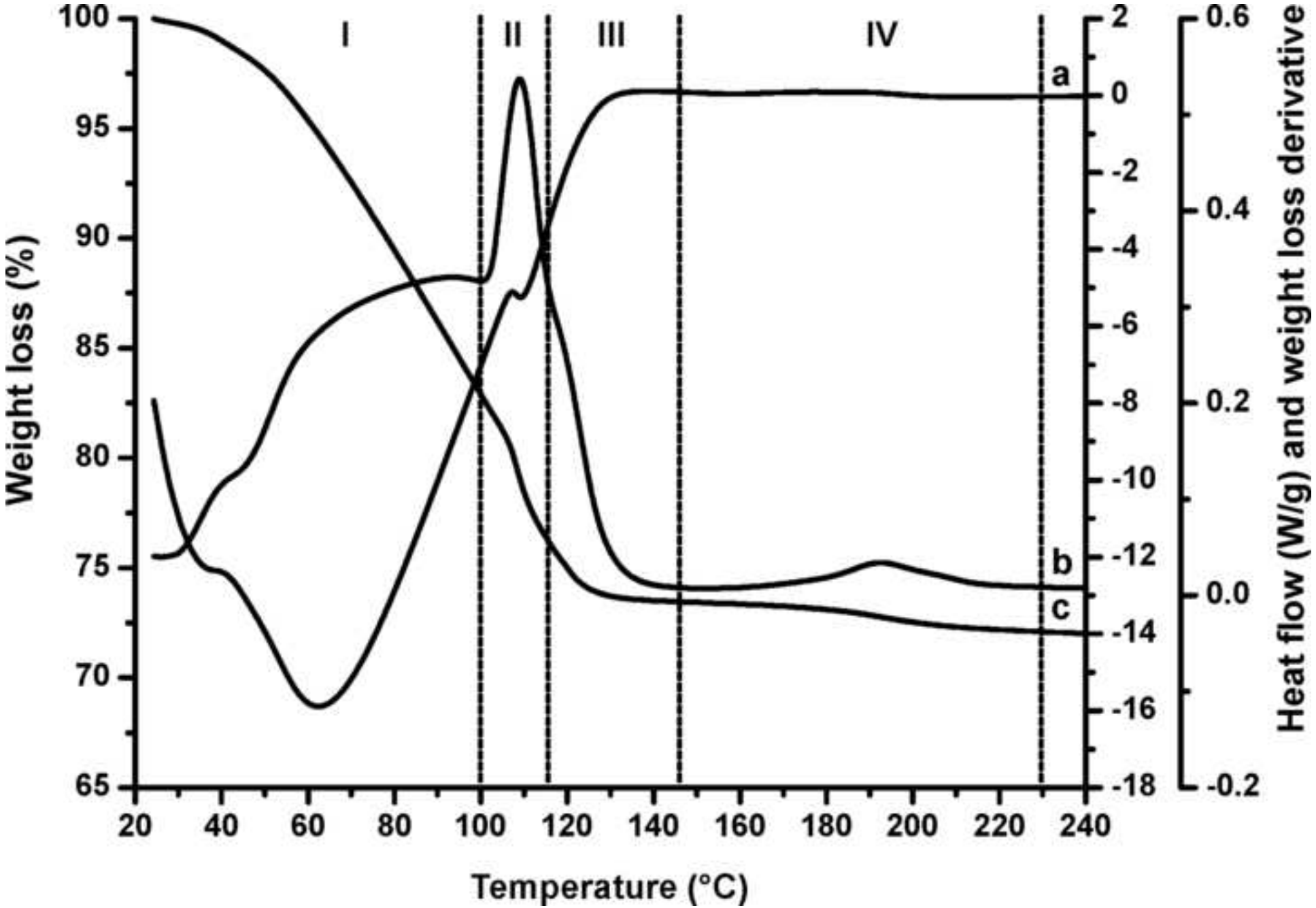

Figure 6

Click here to download high resolution image

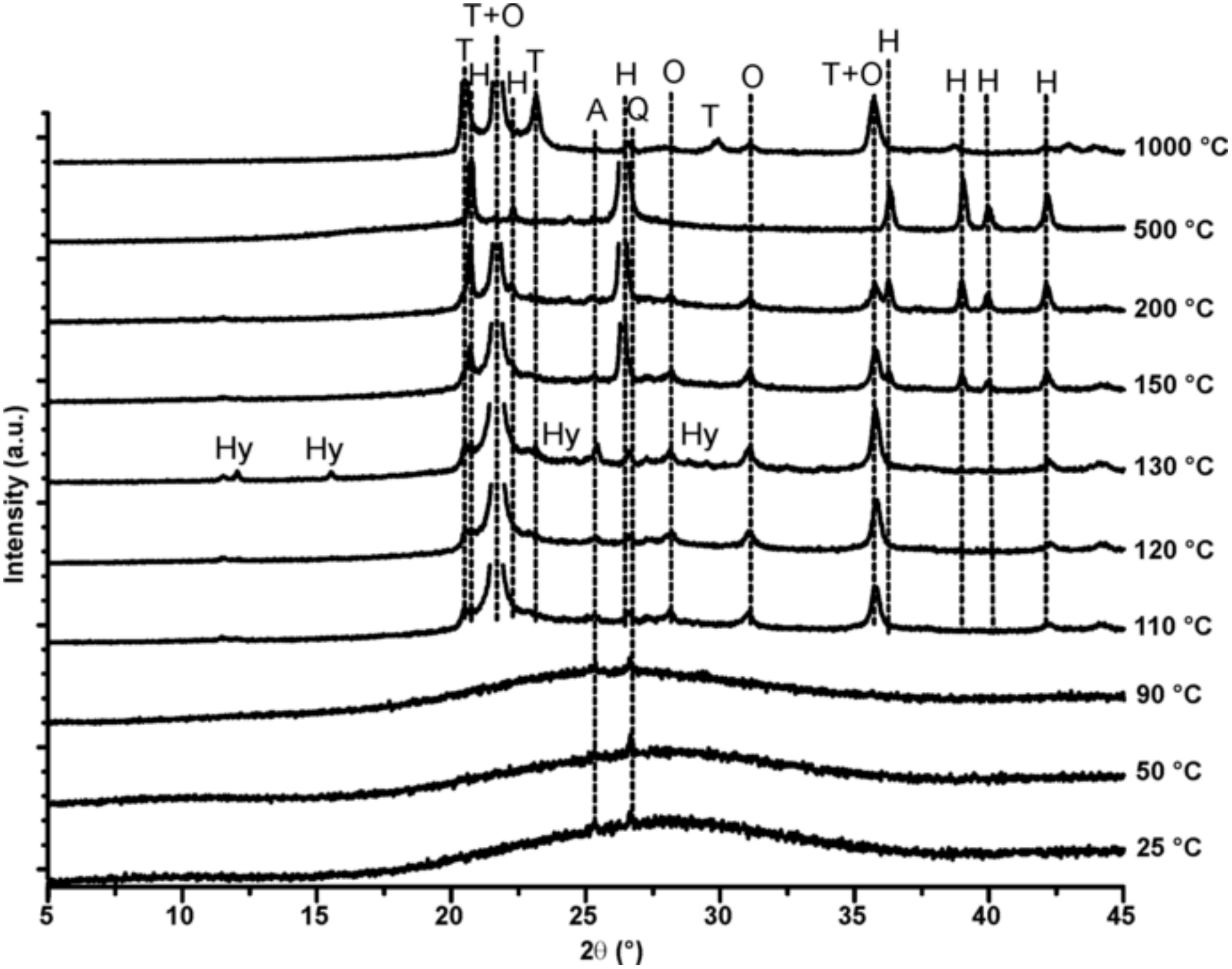

Figure 7

Click here to download high resolution image

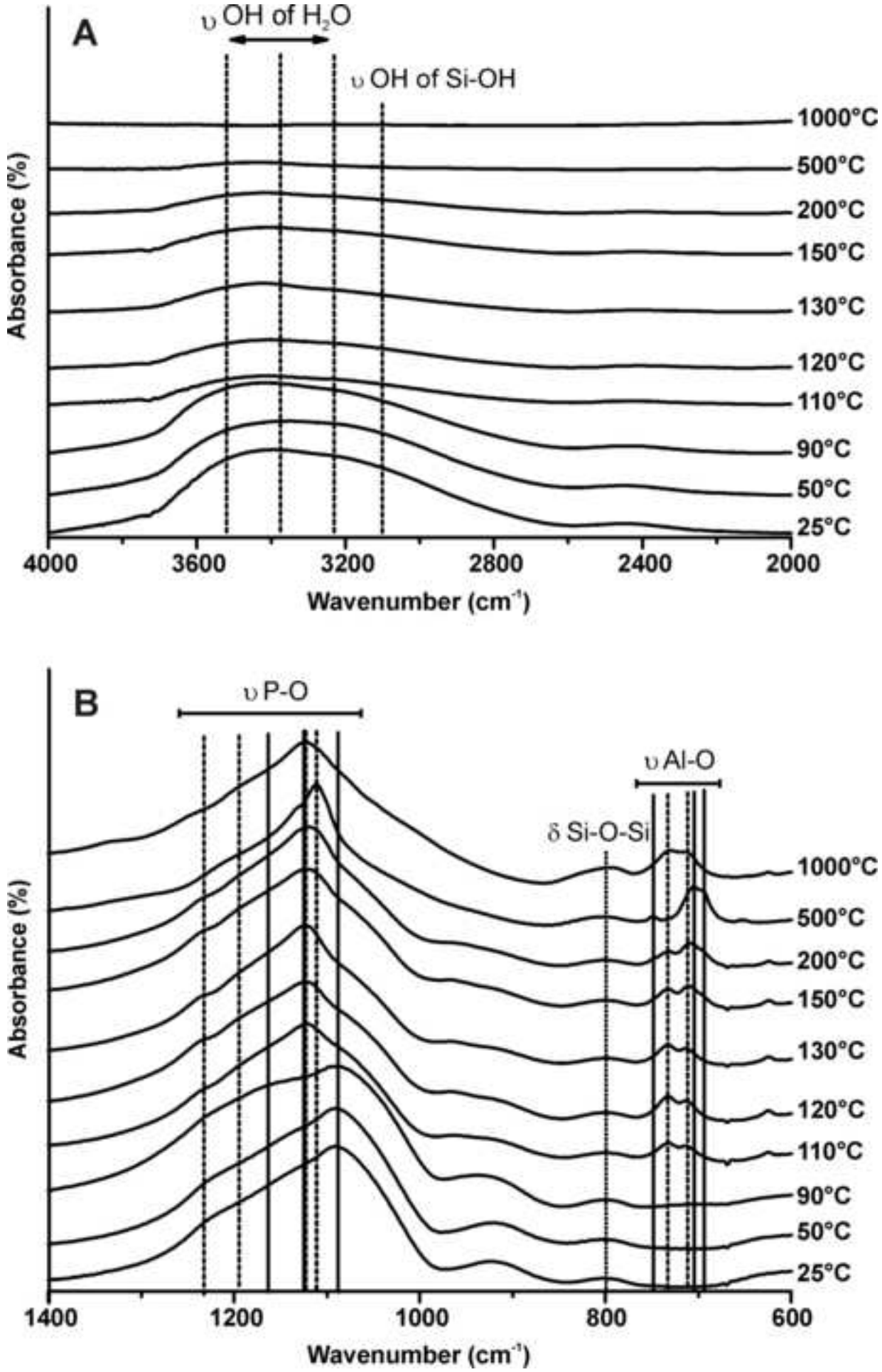

Figure 8

Click here to download high resolution image

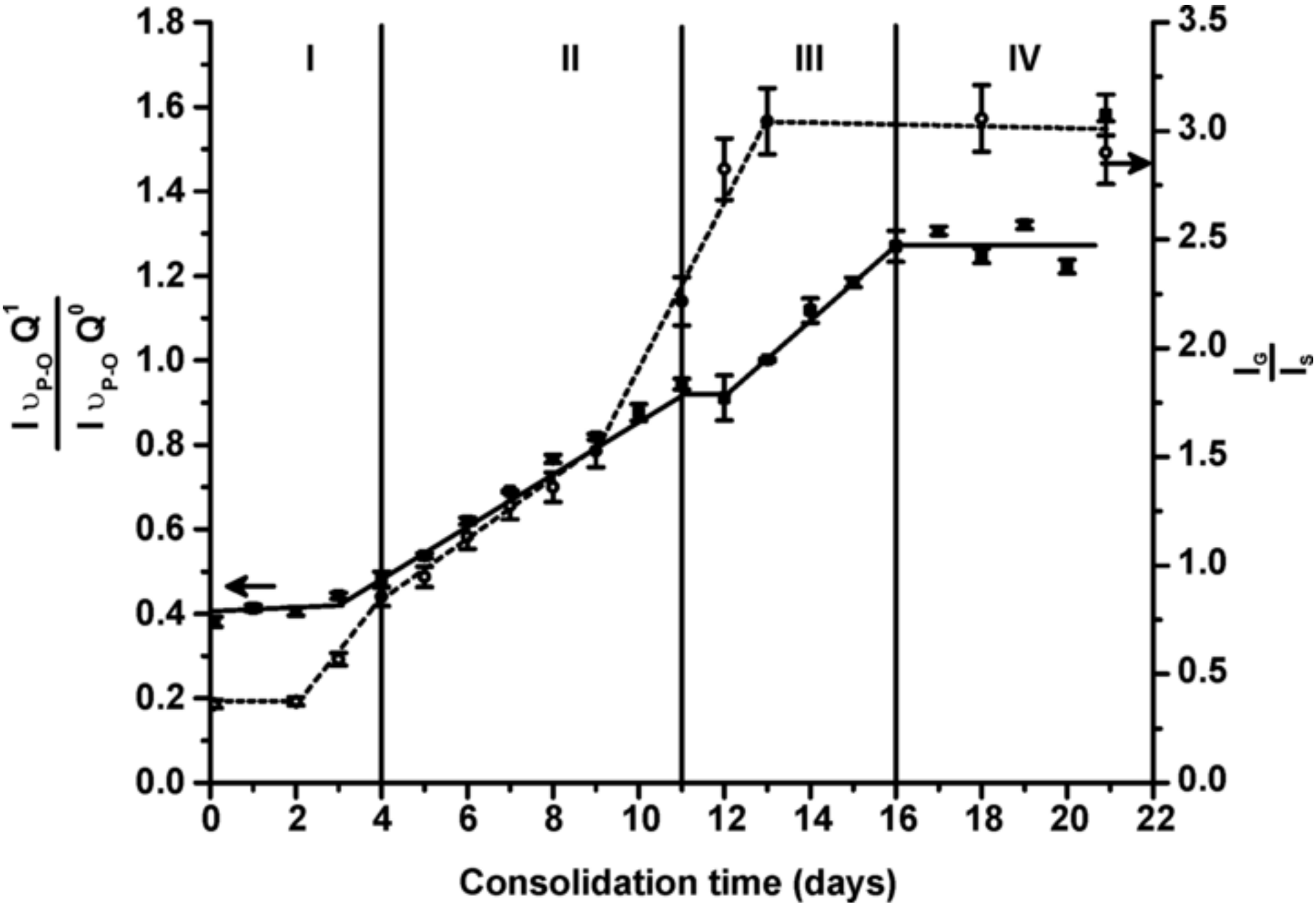

Figure 9

Click here to download high resolution image